Non-Gaussianities and the large $|\eta|$ approach to inflation

Gianmassimo Tasinato[1,2,*]

[1]*Physics Department, Swansea University, SA28PP, United Kingdom*
[2]*Dipartimento di Fisica e Astronomia, Università di Bologna,*
and INFN, Sezione di Bologna, I.S. FLAG, viale B. Pichat 6/2, 40127 Bologna, Italy

The physics of primordial black holes can be affected by the non-Gaussian statistics of the density fluctuations that generate them. Therefore, it is important to have good theoretical control of the higher-order correlation functions for primordial curvature perturbations. By working at leading order in a $1/|\eta|$ expansion, we analytically determine the bispectrum of curvature fluctuations for single field inflationary scenarios producing primordial black holes. The bispectrum has a rich scale and shape dependence, and its features depend on the dynamics of the would-be decaying mode. We apply our analytical results to study gravitational waves induced at second order by enhanced curvature fluctuations. Their statistical properties are derived in terms of convolution integrals over wide momentum ranges, and they are sensitive on the scale and shape dependence of the curvature bispectrum we analytically computed.

I. INTRODUCTION AND CONCLUSIONS

The lack of direct detection of particle dark matter motivates the study of primordial black holes (PBHs) [1–4] as dark matter candidate. Primordial black holes are formed by the collapse of density fluctuations produced during cosmic inflation. See, e.g., [5–11] for reviews. In order for producing PBHs, the size of the inflationary curvature fluctuation spectrum should increase by several orders of magnitude from large towards small scales. This condition can be achieved by models of inflation violating the standard slow-roll conditions, at least during a short epoch within the inflationary process (see, e.g., [12] for an introduction to standard slow-roll inflation). In the simplest PBH-forming scenarios, while the parameter ϵ remains small, the absolute value of the parameter η becomes well larger than one during a short range $\Delta N_{\rm NSR}$ of inflationary e-folds. Typically, since we cannot rely on a perturbative slow-roll expansion, the analysis of such non-slow-roll models requires the use of numerical techniques—although interesting specific scenarios exist, which are amenable of analytic investigation: see, e.g., [13–21].

The work [22] proposes a new perturbative framework based on an expansion in inverse powers of a small parameter $1/|\eta|$. Let us assume that the quantity $|\eta|$ is very large. At the same time, the duration of non-slow-roll phase $\Delta N_{\rm NSR}$ is infinitesimally small, while the value for the product $|\eta|\Delta N_{\rm NSR}$ is kept finite. Cosmological observables based on correlators of curvature perturbations can be then calculated analytically, leading to formulas organized in a $1/|\eta|$ expansion. There is hope that the results of these calculations share general features with the statistics of curvature perturbations computed within more general (and realistic) families of PBH-forming scenarios, characterized by finite values of $|\eta|$. There are interesting analogies with other approaches developed within quantum field theory, as 't Hooft $1/N$ expansion [23]. In such a framework, the large N limit of $SU(N)$ gauge theories is able to shed light on the properties of quantum chromodynamics, characterized by $N = 3$ (see, e.g., [24] for a pedagogical introduction to the subject).

The scope of this work is to analyze more systematically features of non-Gaussian correlators using the large $|\eta|$ approach to single field inflation, going beyond the investigations started in [22]. Primordial non-Gaussianities can be generated in scenarios producing PBHs in inflation, see, e.g., [25–30]. They play an important role in the physics of primordial black holes, since the formation of compact objects depends on the statistics of curvature fluctuations and their probability distribution function, see, e.g., [31–55]. It is then important to have a good analytical control of the properties of the primordial bispectrum in PBH models. After a brief review of the motivations and tools for carrying on a $1/|\eta|$ expansion—see Sec. II, based on [22]—we focus in Sec. III on computing the bispectrum. We discuss the properties of the three point functions of curvature perturbations. Interestingly, our approach allows

[*]g.tasinato2208@gmail.com

us to determine the leading contributions of the third order interactions Hamiltonian, and leads us to analytically compute the bispectrum at leading order in a $1/|\eta|$ expansion. The result depends on a *single* free parameter, which controls the enhancement of the spectrum from large towards small scales. We nevertheless find a very rich scale and shape dependence, which we analyze in detail. Depending on the scale, the bispectrum can be enhanced on an equilateral shape, or on more elongated shapes. In the squeezed limit, the bispectrum satisfies the Maldacena consistency relation, while in a not-so-squeezed regime it can enhance the effects of the non-slow-roll era. For the equilateral shape, the scale dependence of the bispectrum unexpectedly resembles the profile found in Sec. II for the power spectrum. We interpret such behaviors as due to the dynamics of the would-be decaying mode, which affects in similar ways both the two and three point functions for curvature fluctuations.

Armed with these analytical results, we study in Sec. IV specific observables that are sensitive to the shape and scale dependence of the bispectrum. We focus on correlation functions involving scalar induced gravitational waves. Gravitational wave tensor modes can be sourced at second order in perturbations by scalar fluctuations amplified at small scales. The amplitude and properties of the induced tensor fluctuations can be computed in terms of convolution integrals, involving the statistics of the scalar modes sourcing them. Such convolution integrals are sensitive to the properties of curvature fluctuations at all scales, not only on scales nearby the peak of the curvature power spectrum. See, e.g., [56–63] for some of the original papers, [64,65] for discussions on gauge issues on this framework, and [66] for a comprehensive review (and references therein). The primordial non-Gaussianity of curvature fluctuations can affect the correlation functions of induced gravitational waves [67–74]. Most studies in the literature assume a local form for primordial non-Gaussianity. It is important to extend the analysis to more realistic cases of full bispectra computed in specific scenarios, as the ones we determine in Sec. III. In fact, a good knowledge of the shape and scale dependence of the scalar bispectrum through all scales is essential when evaluating convolution integrals. We consider a non-Gaussian observable correlating two (induced) tensor and one scalar mode. Such an observable, in the squeezed limit, plays a role for the multimessenger cosmology proposal pushed forward in [75]. We find an analytical expression for this quantity. The resulting induced non-Gaussianity has a strong scale dependence in the squeezed configuration, with features enhanced around the position of the peak of the induced tensor power spectrum. The overall magnitude of the result is small, but our findings set the stage for more complete analytical studies of the effects of non-Gaussianities of general form in the computations of the statistics of induced gravitational waves.

Our analysis can be extended along several directions. The large $|\eta|$ formalism can be applied to compute the four point function for scalar curvature fluctuations, which can hopefully be reconstructed analytically and unambiguously starting from the fourth order interaction Hamiltonian for perturbations in single field inflation. The result would be important to compute the trispectrum contributions to the induced gravitational wave spectrum (see. e.g.. [71,73,76]), in a realistic setup which includes the complete shape and scale dependence of the quantities involved. Moreover, the large $|\eta|$ approach can be helpful for the ongoing debate of one-loop corrections in PBH-forming scenarios [77,78], which is so far unresolved, see, e.g., [79–92]. In [22] we shown that one loop corrections can be set under control at large scales in the large $|\eta|$ limit, without including the boundary terms later discussed in [90] in the context of loop corrections (but see also [92]). Once the debate on the correct way to carry on the computations will be fully clarified, a consistent analytical investigation in the large $|\eta|$ limit will certainly be instructive.

II. MODE FUNCTIONS AND CURVATURE POWER SPECTRUM

Consider an inflationary scenario that undergoes a brief, but drastic phase of slow-roll violation. The cosmic evolution corresponds to quasi–de Sitter expansion, with a spacetime characterized by a conformally flat Friedmann-Lemaitre-Robertson-Walker metric,

$$ds^2 = a^2(\tau)(-d\tau^2 + d\vec{x}^2). \quad (2.1)$$

The scale factor is $a(\tau) \simeq -1/(H_0\tau)$ for negative conformal time, and nearly constant Hubble parameter H_0. Inflation occurs at negative conformal time, and ends at $\tau = 0$. The first slow-roll parameter $\epsilon = -d\ln H/(d\ln a)$ remains small. But it decreases rapidly during a short phase of non-slow-roll evolution, during which the second slow-roll parameter $\eta = d\ln \epsilon/d\ln a$ is negative and large in absolute value. Scenarios of ultra-slow-roll inflation [93–95] where $\eta = -6$ represent typical situations where the $|\eta|$ parameter is well larger than one for a brief period. They are widely used when discussing the physics of primordial black holes (see, e.g.,[11] for a review on model building). Other scenarios are constant roll models [96–98], and include specific constructions with arbitrarily large values of $|\eta|$, see e.g. [99]. In this work, following [22], we formally consider a case in which $|\eta|$ is large, and at the same time the duration of non-slow-roll phase is brief. We indicate with τ_1 and τ_2, respectively, the (negative) conformal times when the non-slow-roll phase starts and ends. We define the combination

$$\Delta\tau = -\frac{\tau_2 - \tau_1}{\tau_1}, \quad (2.2)$$

and consider the large $|\eta|$ limit:

$$|\eta| \to \infty \quad \text{and} \quad \Delta\tau \to 0,$$

$$\text{while } |\eta|\Delta\tau = \frac{\Pi_0}{2} \text{ remains finite.} \qquad (2.3)$$

The quantity η is computed at the onset of the non-slow-roll phase. This limit is well defined, and leads to meaningful expressions for physical quantities. The latter depend on the single parameter Π_0, which encapsulates all the effects of the brief non-slow-roll era. The condition (2.3) suggests a consistent perturbative expansion in inverse powers of $|\eta|$: whenever we find a $\Delta\tau$ in our formulas, we substitute it with $\Pi_0/(2|\eta|)$ following the prescription of Eq. (2.3), to then perform an expansion in the small $1/|\eta|$ parameter. In analogy with 't Hooft large N expansion [23], we dub the limit of Eq. (2.3) *inflationary large $|\eta|$ expansion* (see [22] for details).

The physical quantities we will be interested in are correlators of primordial fluctuations. We define a dimensionless quantity

$$-k\tau_1 = \kappa \qquad (2.4)$$

combining the Fourier scale k with the conformal time τ_1 around which the non-slow-roll era occurs. The value $\kappa \sim \mathcal{O}(1)$ is the typical scale of modes leaving the horizon during the non-slow-roll era. The evolution of the scalar curvature perturbation $\zeta_\kappa(\tau)$ in Fourier space obeys the Mukhanov-Sasaki equation (see, e.g., [12] for a textbook discussion).

As anticipated above, we assume that the evolution satisfies slow-roll conditions up to a brief phase $\tau_1 \le \tau \le \tau_2$. In the limit of small $\Delta\tau$, the expression for the mode functions can be found analytically [18]. See Appendix A for a review. Starting from formulas (A14)–(A16), and taking the limit (2.3), we find the solution for the mode function satisfying the Mukhanov-Sasaki equation at times $\tau_2 \le \tau \le 0$ after the non-slow-roll phase ends:

$$\zeta_\kappa(\tau) = -\frac{iH_0(-\tau_1)^{3/2}}{2\sqrt{\epsilon_1}\kappa^{3/2}} e^{i\kappa\tau/\tau_1}\left(1 - \frac{i\kappa\tau}{\tau_1}\right)$$
$$- \frac{iH_0(-\tau_1)^{3/2}\Pi_0}{2\sqrt{\epsilon_1}\kappa^{5/2}} e^{2i\kappa - \frac{i\kappa\tau}{\tau_1}}\left[(1-i\kappa)\left(1 + \frac{i\kappa\tau}{\tau_1}\right) + e^{-2i\kappa + \frac{2i\kappa\tau}{\tau_1}}(1+i\kappa)\left(1 - \frac{i\kappa\tau}{\tau_1}\right)\right], \qquad (2.5)$$

where ϵ_1 is the constant, small parameter defined in the first phase of inflationary slow-roll evolution $\tau \le \tau_1$. All of the effects in the mode functions of a non-slow-roll, large $|\eta|$ era are contained in the parameter Π_0 defined in Eq. (2.3), which multiplies the second line of Eq. (2.5).

Starting from Eq. (2.5), we review for the rest of this section some of the results of [22] on the power spectrum of the curvature perturbation, evaluated at the end of inflation $\tau = 0$. In the next section, then, we analyze the bispectrum. The power spectrum at the end of inflation is defined in terms of two point correlators of curvature perturbation,

$$\langle \zeta_\kappa(\tau=0)\zeta_\rho(\tau=0)\rangle = \delta(\vec{\kappa}+\vec{\rho})P_\kappa. \qquad (2.6)$$

At very large scales, $\kappa \ll 1$, the power spectrum acquires the usual scale invariant limit,

$$P_{\kappa \ll 1}(\tau) = \frac{\mathcal{P}_0}{\kappa^3}, \quad \text{with} \quad \mathcal{P}_0 = \frac{H_0^2(-\tau_1)^3}{4\epsilon_1}. \qquad (2.7)$$

However, at smaller scales, the structure of the mode function (2.5) leads to a rich scale dependence for the two point function. We define the dimensionless spectrum evaluated at the end of inflation,

$$\Pi(\kappa) = \frac{P_\kappa(\tau=0)}{P_{\kappa \ll 1}(\tau=0)}, \qquad (2.8)$$

as a ratio between values of the spectrum at scale κ, versus the spectrum at $\kappa = 0$. Equation (2.5) leads to

$$\Pi(\kappa) = 1 + 4\Pi_0\kappa j_1(\kappa)(\kappa j_1(\kappa) - j_0(\kappa)) + 4\Pi_0^4\kappa^2 j_0^2(\kappa), \qquad (2.9)$$

where

$$j_0(\kappa) = \frac{\sin\kappa}{\kappa}; \qquad j_1(\kappa) = \frac{\sin\kappa}{\kappa^2} - \frac{\cos\kappa}{\kappa} \qquad (2.10)$$

are the spherical Bessel functions. The profile for the function $\Pi(\kappa)$ is represented in Fig. 1. As anticipated, in the limit of infinitely large $|\eta|$, the $1/|\eta|$ corrections vanish and the resulting spectrum depends only on one parameter, Π_0. Corrections of order $1/|\eta|$ and higher can be computed starting with formulas of Appendix A. They improve the small scale behavior reducing the amplitude of oscillations for $\kappa > 1$ in Fig. 1, but they do not affect the large scale profile $\kappa \le 1$. It is clear that the amplitude of the spectrum increases considerably from large towards small scales, reaching its maximal values starting around $\kappa \sim \mathcal{O}(1)$. In fact, the parameter Π_0 in Eq. (2.3) has a transparent physical interpretation, since it controls the amplification
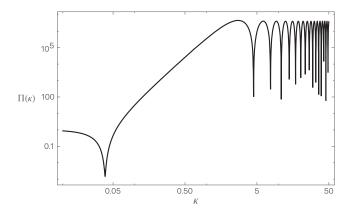
FIG. 1. The quantity $\Pi(\kappa)$ introduced in Eq. (2.8), evaluated for $\Pi_0 = 10^3$.

of the spectrum between large and small scales (see [22] and Appendix A):

$$\frac{\lim_{\kappa \to \infty} P_\kappa(\tau = 0)}{\lim_{\kappa \to 0} P_\kappa(\tau = 0)} = (1 + \Pi_0)^2. \qquad (2.11)$$

If we wish a large value of $\Pi(\kappa)$ at small scales, as required in models leading to primordial black hole formation, then the value of the parameter Π_0 should be large. We assume this condition in what follows.

What is causing the rich scale dependence of the curvature spectrum, as represented in Fig. 1? The would-be decaying mode is responsible, and does not actually decay at superhorizon scales during the phase of non-slow-roll evolution. It is the disruptive interference between decaying and nondecaying mode that produces the dip in the spectrum at intermediate scales, which is clearly visible in Fig. 1. Moreover, also the rapid growth in the spectrum from large towards small scales (scaling with a slope κ^4 [100]) is caused by the decaying mode dynamics. See, e.g., [11] for a review.

With the aid of our analytical formulas, it is not difficult to analytically determine the position of the dip in scenarios with large Π_0. We assume that the position of the dip is parametrized as $\kappa = x\sqrt{3/(2\Pi_0)}$, with x some dimensionless constant to be determined. We plug this ansatz in (2.9), and expand the result for large Π_0. We find the expression

$$\Pi(x) = (1 - x)^2 + \frac{3x^4(6 - x^2)}{10\Pi_0} + \mathcal{O}\left(\frac{1}{\Pi_0^2}\right). \qquad (2.12)$$

The position of the dip in the spectrum corresponds to a choice of x which makes the first contribution in the previous formula vanishing, leaving us with the remaining small contributions suppressed by powers of the small quantity $(1/\Pi_0)$. This leads to the choice $x = 1$, hence,

$$\kappa_{\text{dip}} = \sqrt{\frac{3}{2\Pi_0}}; \qquad \Pi(\kappa_{\text{dip}}) = \frac{3}{2\Pi_0} + \mathcal{O}\left(\frac{1}{\Pi_0^2}\right). \qquad (2.13)$$

Comparing formulas (2.11) and (2.13), we learn that the position of the dip with respect to the peak is proportional to the inverse fourth power of the total gain in magnitude of the spectrum from large to small scales [18]. The single parameter Π_0 hence characterizes the spectrum and all its features.

The overall properties of the curvature spectrum we determined with the large $|\eta|$ approach to inflation are in common with several inflationary models leading to primordial black hole production, based on violations of slow-roll conditions. Various other analytical studies are based on different approaches, see, e.g., [13,14,16–21]. Our formulas have the nice feature of depending on a single parameter Π_0, with a clear physical interpretation. Moreover, the large $|\eta|$ approach is sufficiently flexible to be straightforwardly applicable to the computation of three point functions for curvature fluctuations, leading to novel analytical results for the bispectrum. We explore this topic in what comes next.

III. LARGE $|\eta|$ LIMIT AND NON-GAUSSIANITIES

In the previous section, we showed how the large $|\eta|$ approach of limit (2.3) leads to a simple analytical expression for the power spectrum in Eq. (2.9). It depends on a single dimensionless parameter Π_0, and it has clear physical properties matching what was found in more sophisticated inflationary models of primordial black holes. In this section, we study the implication of Eq. (2.3) for the curvature three point function and the associated bispectrum. The topic was briefly discussed in [22]. Here we investigate it more systematically. We will be able to determine fully analytical formulas for the bispectrum, including its scale and shape dependence, depending again on the single free parameter Π_0 introduced in (2.3).

It is well known that non-Gaussianities in the statistics of fluctuations can play an important role in the formation of primordial black holes from inflation, for example since it affects the estimates of the threshold of PBH formation. See, e.g., [31–34,36–45,48–54] for works studying different aspects of this topic. In many studies, it is customary to consider primordial non-Gaussianity with a local form. In this work we analytically compute the bispectrum from first principles using the in-in formalism, in the large $|\eta|$ limit of inflation. We show that non-Gaussian features are characterized by a rich shape and scale dependence.

Our assumptions for the behavior of the system—quasi–de Sitter slow-roll expansion throughout the inflationary era, a part from a brief phase of large $|\eta|$ evolution—help us to uniquely characterize the structure of the curvature three point function. The third order interaction Hamiltonian for

curvature perturbations in single field inflation [101] contains *one* term which gives the dominant contribution to the bispectrum [77,78],

$$\mathcal{H}_{\text{int}}(\tau) = -\frac{1}{2} \int d^3 x a^2(\tau) \epsilon(\tau) \eta'(\tau) \zeta^2(\tau, \vec{x}) \zeta'(\tau, \vec{x}). \quad (3.1)$$

Since this contribution depends on the time derivative $\eta'(\tau)$, it is proportional to the large jump in the η parameter occurring at the beginning ($\tau = \tau_1$) and at the end ($\tau = \tau_2$) of the non-slow-roll phase. Since this epoch is extremely brief in our framework, we have no option but to consider a *sudden transition* among different evolution eras. We can then express the time derivative of the η parameter, as appearing in Eq. (3.1), as [78]

$$\eta'(\tau) = \Delta\eta[-\delta(\tau - \tau_1) + \delta(\tau - \tau_2)], \quad (3.2)$$

the quantity $\Delta\eta$ in Eq. (3.2) controls the jump of the η parameter. We will soon determine its precise value, making use of appropriate physical arguments.

But first, we use the interaction Hamiltonian (3.1) to write a formal expression for the bispectrum B_ζ at the end of inflation, $\tau = 0$, defined by means of the formula:

$$\langle \zeta_{\kappa_1}(0) \zeta_{\kappa_2}(0) \zeta_{\kappa_3}(0) \rangle = \delta(\vec{\kappa}_1 + \vec{\kappa}_2 + \vec{\kappa}_3) B_\zeta(\kappa_1, \kappa_2, \kappa_3). \quad (3.3)$$

As usual, momentum conservation requires that the vectors labeling the perturbations in Fourier space form a closed triangle. The in-in formalism prescribes to compute the three-point correlator as

$$\langle \text{in} | \bar{T} e^{-i \int \mathcal{H}_{\text{int}}(\tau') d\tau'} \zeta_{\kappa_1}(0) \zeta_{\kappa_2}(0) \zeta_{\kappa_3}(0) T e^{i \int \mathcal{H}_{\text{int}}(\tau') d\tau'} | \text{in} \rangle. \quad (3.4)$$

Using the ansatz (3.2), we obtain the following structure [78]:

$$B_\zeta(\kappa_1, \kappa_2, \kappa_3) = -2\Delta\eta(\epsilon(\tau_2)a^2(\tau_2)\text{Im}[(\zeta_{\kappa_1}(0)\zeta^*_{\kappa_1}(\tau_2))(\zeta_{\kappa_2}(0)\zeta^*_{\kappa_2}(\tau_2))(\zeta_{\kappa_3}(0)\partial_{\tau_2}\zeta^*_{\kappa_3}(\tau_2))] - (\tau_2 \to \tau_1)) + \text{perms.} \quad (3.5)$$

To proceed with the computations, we now determine the value of $\Delta\eta$ in Eq. (3.5).

A. The value of $\Delta\eta$, and the resulting structure of the bispectrum

We start computing the squeezed limit of the expression (3.5). Formally it reads

$$\lim_{q \to 0} B_\zeta(\kappa, \kappa, q) = -4\Delta\eta\epsilon(\tau_2)a^2(\tau_2)|\zeta_q(0)|^2|\zeta_\kappa(0)|^2$$

$$\times \left\{ \text{Im}\left[\frac{\zeta_\kappa^2(0)}{|\zeta_\kappa(0)|^2}\zeta^*_\kappa(\tau_2)(\zeta'_\kappa(\tau_2))^*\right] - \frac{\epsilon(\tau_1)a^2(\tau_1)}{\epsilon(\tau_2)a^2(\tau_2)}\text{Im}\left[\frac{\zeta_\kappa^2(0)}{|\zeta_\kappa(0)|^2}\zeta^*_\kappa(\tau_1)(\zeta'_\kappa(\tau_1))^*\right] \right\}. \quad (3.6)$$

In the absence of a phase of slow-roll violation, the squeezed limit of the previous formula satisfies the Maldacena consistency relation [101]:

$$\lim_{q \to 0} B(\kappa, \kappa, q) = -(n_\zeta(\kappa) - 1)|\zeta_q(0)|^2|\zeta_\kappa(0)|^2, \quad (3.7)$$

with $(n_\zeta(\kappa) - 1) = d\ln\Pi(\kappa)/d\ln\kappa$. In our case, we can expect the consistency relation (3.7) to be satisfied for small κ, in a regime $q \ll \kappa \ll 1$. In fact, modes with such small values of momenta leave the horizon early in the inflationary phase, well before the non-slow-roll epoch occurs. Correspondingly, the decaying mode has a long time to decay: it cannot be significantly resurrected by the non-slow-roll phase, which occurs much later than its horizon crossing. We can then plug the mode functions determined in Appendix A into Eq. (3.6). We expand for small κ, and we impose the validity of (3.7) up to order κ^2. This procedure determines uniquely the parameter $\Delta\eta$ in the large $|\eta|$ limit of Eq. (2.3). We find

$$\Delta\eta = \frac{|\eta|}{(1 + \Pi_0)} + \frac{\Pi_0(12 + 34\Pi_0 + 25\Pi_0^2)}{2(1 + \Pi_0)^2(1 + 2\Pi_0)}, \quad (3.8)$$

up to corrections of order $1/|\eta|$.

Armed with the precise value of $\Delta\eta$, as well as with the mode functions computed in Appendix A, we can analytically evaluate the full bispectrum using Eq. (3.5). The overall coefficient (proportional to $\Delta\eta$) scales as $|\eta|$. Taking differences over mode functions within the parentheses of (3.5), we find that they scale as $1/|\eta|$, compensating for the overall large factor $|\eta|$. Taking the limit (2.3) of large $|\eta|$ we obtain a finite, well defined result for the bispectrum. Its structure is

$$B_\zeta(\kappa_1, \kappa_2, \kappa_3) = \mathcal{P}_0^2 \mathcal{A}_\zeta(\kappa_1, \kappa_2, \kappa_3), \quad (3.9)$$

with $\mathcal{P}_0$ given in Eq. (2.7), while the dimensionless function $\mathcal{A}$ is built in terms of the combination

$$\mathcal{A}_\zeta(\kappa_1, \kappa_2, \kappa_3) = \sum_{n=1,\ldots,4} \mathcal{C}_n(\kappa_1, \kappa_2, \kappa_3)\Pi_0^n. \qquad (3.10)$$

The analytical expression for the functions $\mathcal{C}_n$ can be found in Appendix B. They are oscillatory functions of combinations of momenta. The resulting bispectrum has a rich momentum and shape dependence, which we explore in what follows.

B. The squeezed (and not-so-squeezed) limit of the bispectrum

The squeezed limit of the bispectrum (3.9) can be studied analytically. It satisfies the Maldacena consistency relation *for any value of* κ. Defining

$$\lim_{q\to 0}\mathcal{A}(\kappa, \kappa, q) = \frac{6}{5} f_{\rm NL}^{\rm sq} \frac{\Pi(\kappa)}{\kappa^3}\frac{\Pi(q)}{q^3}, \qquad (3.11)$$

we have the relation

$$f_{\rm NL}^{\rm sq}(\kappa) = \frac{5}{6}(1 - n_\zeta(\kappa)). \qquad (3.12)$$

See Fig. 2, left panel. This result might appear surprising, since it is well known that the Maldacena consistency relation can be violated in scenarios which include ultra-slow-roll phases (see, e.g., [94,102,103]). Our result of Eq. (3.12) indicates the duration (2.2) of the non-slow-roll era is too brief for triggering a violation of the consistency condition—no matter how large $|\eta|$ is.

As manifest in Fig. 2, left panel, the squeezed limit of the bispectrum is strongly scale dependent, reaching its extrema in the region $\kappa_{\rm dip}$ around the dip in the spectrum, to then assume values of order 1 (and negative) for scale $\kappa \sim \mathcal{O}(1)$ towards the first peak of the spectrum. (See, e.g., [104–106] for early works on scale-dependent non-Gaussianities.) Again, the features of $f_{\rm NL}^{\rm sq}$ are determined by the single parameter Π_0 controlling the spectrum.

Since we have analytical control of the bispectrum, we can also investigate the first order corrections $\mathcal{O}(q^2)$ to the squeezed bispectrum. Such contributions can be associated with the curvature of the background; see, e.g., [107]. They can manifest significant deviations from the predictions of standard slow-roll scenarios. We parametrize such corrections in terms of a function $G(\kappa)$:

$$\lim_{q\ll 1}\mathcal{A}(\kappa, \sqrt{\kappa^2 + q^2}, q) = -(n_\zeta(\kappa) - 1)\frac{\Pi(\kappa)}{\kappa^3}\frac{\Pi(q)}{q^3}$$
$$+ q^2 \frac{\Pi(\kappa)}{\kappa^3}\frac{\Pi(q)}{q^3}G(\kappa) + \mathcal{O}(q^3). \qquad (3.13)$$

In computing the next-to-leading corrections (3.13), we focus on momenta forming a right triangle, with one of the catheti corresponding to the small momentum q. We represent in Fig. 2, right panel, the function $G(\kappa)$ controlling the correction q^2 in Eq. (3.13) (normalized by inverse powers of Π_0). As apparent from the figure, this function has a distinctive feature around the position $\kappa_{\rm dip}$ of the dip of the spectrum. This feature can be interpreted as due to the decaying mode, which influences the dynamics around $\kappa_{\rm dip}$. The amplitude of this feature is parametrically larger by a factor of order $\Pi_0^{3/2}$ with respect to the feature associated with the spectral index and $f_{\rm NL}^{\rm sq}$ (which we represent for comparison in Fig. 2). This indicates that the effects of the would-be decaying mode and of the non-slow-roll phase—controlled by Π_0—become more and more accentuated as we leave the squeezed limit. In fact, we will now find further manifestations of the would-be decaying mode dynamics by studying other shapes of the bispectrum.

C. The equilateral shape of the bispectrum

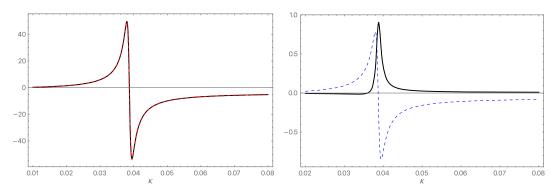For an equilateral bispectrum, where all momenta have the same size κ, we find interesting overlaps between the

FIG. 2.   Left: the squeezed bispectrum satisfies Maldacena consistency relation. Red: $(1 - n_\zeta)$; dashed black: the squeezed nonlinear parameter $5f_{\rm NL}^{\rm sq}/6$ defined in Eq. (3.11). Right: the function $G(\kappa)$ defined in Eq. (3.13), divided by Π_0^2 (black line). The quantity $(ns - 1)/2$ divided by $\Pi_0^{1/2}$ (dashed blue line). The normalization factors are introduced to obtain comparable variables for the two quantities introduced. In both panels, $\Pi_0 = 10^3$.
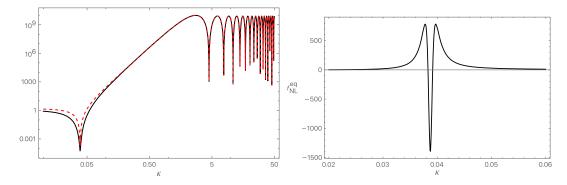
FIG. 3. Left: the right-hand side of Eq. (3.14) (black line) versus the left-hand side of the same equation (dashed red line). Right: the quantity f_{NL}^{eq} defined in Eq. (3.15). In both panels, $\Pi_0 = 10^3$.

scale-dependent profiles of the bispectrum and of the power spectrum. Recall the expressions for the dimensionless quantities $\mathcal{A}$ and Π in Eqs. (3.10) and (2.9). We find the relation

$$\frac{\kappa^4}{6\Pi_0} |\mathcal{A}_\zeta(\kappa,\kappa,\kappa)| \simeq \Pi^{3/2}(\kappa) \qquad (3.14)$$

is very well satisfied for the entire range of scales; see Fig. 3, left panel. Again, we interpret this behavior as due to the dynamics of the decaying mode, which increases the magnitude of the equilateral bispectrum in a similar way as it does for the power spectrum.

As customary, we define the dimensionless parameter f_{NL}^{eq},

$$f_{NL}^{eq}(\kappa) = \frac{5}{18} \frac{B_\zeta(\kappa,\kappa,\kappa)}{P_\kappa^2} = \frac{5}{18} \frac{\kappa^6 \mathcal{A}_\zeta(\kappa,\kappa,\kappa)}{\Pi^2(\kappa)}, \qquad (3.15)$$

controlling the size of the equilateral bispectrum with respect to the power spectrum, and represent its scale-dependent profile in Fig. 3, right panel. The size of f_{NL}^{eq} is relatively small at all scales, a part from the region around $\kappa_{dip} = \sqrt{3/(2\Pi_0)}$, where it develops pronounced features. (See also [108,109] for related computations using a different approach based on [15].)

A very similar behavior occurs for other non-Gaussian shapes as well, and can be studied with our analytic

formula (3.10). To conclude this section, we investigate the shape dependence of the bispectrum using a convenient graphical representation in terms of triangular plots.

D. Graphical representation of more general shapes of the bispectrum

For representing the shape dependence of the bispectrum as a function of the scale, we use the graphical device introduced in [110] (see also [12] for a pedagogical review). We define the function

$$S(\kappa_1,\kappa_2,\kappa_3) = N\kappa_1^2\kappa_2^2\kappa_3^2 B_\zeta(\kappa_1,\kappa_2,\kappa_3), \qquad (3.16)$$

where the normalization constant N is selected such that $S(1,1,1) = 1$. We then introduce the coordinates $x_2 = \kappa_2/\kappa_1$, $x_3 = \kappa_3/\kappa_1$, and represent the magnitude of $S(\kappa,x_2,x_3)$ in triangular plots as in Fig. 4. Ordering momenta such that $x_3 \le x_2 \le 1$, the triangular inequality requires $x_2 + x_3 > 1$. To avoid representing configurations which are equivalent, we only focus on the region $1 - x_2 \le x_3 \le x_2$. Given the fact that our bispectrum is strongly dependent on the scale, the result depends on the choice of the first argument κ in the quantity $S(\kappa,x_2,x_3)$. We make the two choices $\kappa = \kappa_{dip}$ and $\kappa = 1$. While for $\kappa = 1$ the bispectrum is mostly enhanced for the equilateral shape, the behavior at κ_{dip} is more rich, and the spectrum is enhanced for elongated triangles, where the size of two of the momenta is well larger than the third one. Hence, depending on the scales one considered, different
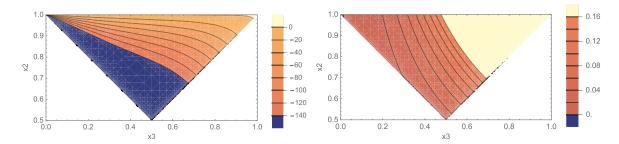

FIG. 4. Triangular plots of the function $S(\kappa,x_2,x_3)$ of Eq. (3.16), represented with the criteria discussed in the text. Left: $S(\kappa_{dip},x_2,x_3)$. Right: $S(1,x_2,x_3)$.

shapes can become dominant, with distinct consequences for observables controlling the physics of PBHs.

In fact, is there any specific physical implication for the rich scale dependence of the bispectrum in our system, as we explored so far? In the next section, we will study some consequences of our findings for the statistics of scalar-induced gravitational waves.

IV. GRAVITATIONAL WAVES AND NON-GAUSSIANITY

In the investigations we carried on so far, we demonstrated that the analytical bispectrum of Eq. (3.10) has a rich shape and scale dependence, more complex than a pure local-type non-Gaussian statistics. The information we obtained can be important when studying observables that involve convolution integrals over all scales. Such quantities can in fact be sensitive to the large scale features of the bispectrum we investigated in Sec. III.

Explicit examples are observables built in terms of tensor modes sourced *at second order* by scalar fluctuations which are enhanced at small scales, for example by non-slow-roll epochs as considered in Secs. II and III. See, e.g., [56–63] for some of the original papers on the subject, [64,65] for discussions on gauge issues on this framework, and [66] (and references therein) for a comprehensive review. Integrations involving convolutions depend on the power spectrum and bispectrum at all scales. They are sensitive to the features of the statistics of fluctuations that we studied in the previous section. In fact, observables relative to the induced tensor two and three point functions constitute an important, although indirect, experimental window on small-scale scalar fluctuations. We proceed to study this phenomenon explicitly.

Schematically, scalar perturbations with an enhanced curvature spectrum $P_\zeta(k)$ [recall its definition in Eq. (2.6)] can source a tensor spectrum P_h at second order in fluctuations,

$$P_h(k) = \int dk' f(k, k') P_\zeta(k') P_\zeta(k - k'), \quad (4.1)$$

where $f(k, k')$ is a kernel function depending on cosmology. For convenience, in this section we make use of dimensionful momenta k: their dimensionless version κ can be easily obtained in terms of the definition (2.4). Expressions as (4.1) are derived under the hypothesis of Gaussian primordial curvature fluctuations. Local type non-Gaussianity can modulate the scale dependence of the induced tensor spectrum, with interesting phenomenological implications [67–74]. Here we explore the implications of an enhanced curvature bispectrum for another interesting observable: the tensor-tensor-scalar bispectrum B_{TTS} evaluated during radiation domination. The quantity B_{TTS} involves two (scalar induced) tensor modes h and one Bardeen scalar mode Φ. Schematically, in the squeezed

limit we expect a relation like the following one (soon we will be more precise):

$$B_{\text{TTS}}(k_1, k_2, k_3) = \int dq \tilde{f}(k_1, k_2, q) B_\zeta(k_1, k_2, q) P_\zeta(k_1 - q), \quad (4.2)$$

for $\tilde{f}$ some kernel function. A squeezed version of the bispectrum of Eq. (4.2) can correlate (scalar induced) stochastic backgrounds probed by gravitational wave experiments at small scales, with large scale scalar modes probed by cosmic microwave background observations. It is the observable investigated in [75] (see also [111–119]) for carrying on a "multimessenger cosmology" program. It suggests new experimental avenues for probing the physics of the early Universe, and its detection and characterization would provide a smoking gun for the primordial origin of the gravitational stochastic background. Besides the squeezed limit, the bispectrum B_{TTS} might be phenomenologically relevant for other elongated shapes also, above all if its size is large.

We leave these interesting phenomenological applications aside, and we proceed with computing more precisely the observable B_{TTS} described above Eq. (4.2). The actual computations are rather technical, and we relegate them to Appendix C. Let us start discussing the results for the squeezed limit, where expressions simplify. We find ($k_1 = k_2 = k$)

$$\lim_{k_3 \to 0} B_{\text{TTS}}(k, k, k_3) = \frac{12}{5} f_{\text{NL}}^{\text{TTS}}(k) P_h(k) P_\zeta(k_3), \quad (4.3)$$

where

$$f_{\text{NL}}^{\text{TTS}}(\tau, k) \equiv \frac{5}{12} \frac{\int d^3 q P_\zeta(|\vec{k} - \vec{q}|) P_\zeta(q) [1 - n_\zeta(q)] \mathcal{F}_0(\tau, \vec{k}, \vec{q})}{\int d^3 q P_\zeta(|\vec{k} - \vec{q}|) P_\zeta(q) \mathcal{F}_0(\tau, \vec{k}, \vec{q})}, \quad (4.4)$$

while the tensor spectrum is

$$P_h(\tau, k) = \int d^3 q P_\zeta(|\vec{k} - \vec{q}|) P_\zeta(q) \mathcal{F}_0(\tau, \vec{k}, \vec{q}). \quad (4.5)$$

The explicit expression for the kernel function $\mathcal{F}_0$ can be found in Eq. (C12). In writing Eq. (4.4) we use the fact that the squeezed limit of the scalar bispectrum satisfies the Maldacena consistency relation, see Sec. III.

Starting from Eq. (4.5) it is straightforward to derive the expression for the gravitational wave energy density Ω_{GW}, and perform the integrals numerically by implementing the convenient formulas of [120]. We represent the result in Fig. 5, left panel, where we compute the Ω_{GW} induced by the analytical scalar spectrum of Eq. (3.9). To avoid numerical issues, we smoothed out the oscillatory features
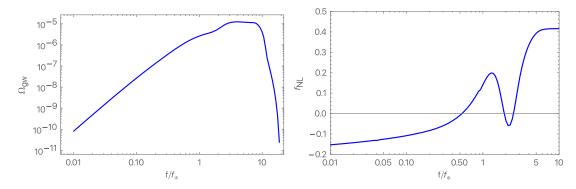
FIG. 5. Left: plot of the gravitational wave energy density induced by a scalar spectrum derived from Eq. (4.5), with $\Pi_0 = 10^3$, under the conditions discussed in the main text. Right: plot of the nonlinear parameter $f_{\rm NL}^{\rm TTS}$ in Eq. (4.4) computed with the same curvature spectrum of the left figure.

occurring at small scales $\kappa > 1$, and we truncated the power at $\kappa = 10$ [i.e. we set $\Pi(\kappa) = 0$ for $\kappa > 10$]. We converted to frequency $f = 2\pi k$. The result is a broad gravitational spectrum, with an ample plateau for $1 \le f/f_* \le 10$, with f_* a reference frequency. See Fig. 5, left panel. In Fig. 5, right panel, we represent the nonlinear parameter $f_{\rm NL}^{\rm TTS}$ introduced in Eq. (4.4), computed starting from the curvature power spectrum as described above. $f_{\rm NL}^{\rm TTS}$ has a strong dependence on the scale, and its typical magnitude is not large, being of the order of 10^{-1}. It has an oscillatory

behavior of $f_{\rm NL}^{\rm TTS}$ at frequencies around the peak of the tensor spectrum. We interpret it as a consequence of the sign change and amplified features of the scalar spectral index $n_\zeta(\kappa) - 1$ appearing in the integrand of Eq. (4.4) (see Fig. 2), which are amplified where the tensor spectrum is most enhanced. It would be interesting to explore whether other shapes can reach larger magnitudes in this setup.

In fact, the general structure of the $B_{\rm TTS}$ bispectrum is given in Eq. (C16), which we report here:

$$
\begin{aligned}
B_{\rm TTS}(\vec{k}_1, \vec{k}_2, \vec{k}_3) = & \int d^3 q P_\zeta(|\vec{k}_1 - \vec{q}|) B_\zeta(q, |\vec{k}_3 + \vec{q}|, k_3) \mathcal{F}_1(\tau, \vec{k}_1, \vec{k}_3, \vec{q}) \\
& + P_\zeta(k_3) \int d^3 q B_\zeta(|\vec{k}_1 + \vec{k}_3|, |\vec{q} + \vec{k}_1 + \vec{k}_3|, q) \mathcal{F}_2(\tau, \vec{k}_1, \vec{k}_3, \vec{q}),
\end{aligned}
\tag{4.6}
$$

where the quantities $\mathcal{F}_{1,2}$ can be found in Eqs. (C17) and (C18). Such an expression shows that the scale and shape dependence of the bispectrum can play an important role. For example, going beyond the squeezed limit [considering the leading k_3^2 corrections to Eq. (4.3), which might still be relevant for coupling large and small scale modes], the convolution integral in the second line in Eq. (4.6) starts to contribute to the result, in a way that depends on shapes of the bispectrum different from the local one. We learned in Sec. III how the effects of the non-slow-roll phase, and of a large parameter Π_0, can considerably influence the amplitude of the bispectrum for shapes different from local. It will be important to further study the behavior of $B_{\rm TTS}$ for general shapes and its phenomenological consequences.

While in this work we focused on the bispectrum, the large $|\eta|$ approach can also be applied to compute the trispectrum at leading order in $1/|\eta|$. We are hopeful that, starting from the fourth order interaction Hamiltonian, and proceeding as in Sec. III, a full analytic expression for the scalar trispectrum can be determined. We expect such an expression to exhibit a rich shape and scale dependence, as

we found for the bispectrum. Such a result would be relevant for the computation of the induced spectrum of gravitational waves, which through convolution integrals is modulated by the trispectrum [71,73,76]. While most of the works so far focused on local type non-Gaussian correlators, it would be interesting to extend computations to the case of a more complex trispectrum derived from first principle calculations in the $1/|\eta|$ limit.

APPENDIX A: THE MODE FUNCTIONS DURING THE BRIEF NON-SLOW-ROLL PHASE

In this Appendix we briefly review the results of [18] which analytically compute the solution for mode functions in a scenario of inflation undergoing a brief, but drastic,

phase of non-slow-roll evolution. We parametrize the background evolution as constituted by three phases:

(1) An initial slow-roll phase, where the slow-roll parameters ϵ and η are very small and the evolution can be approximated as de Sitter phase. The constant value of the parameter ϵ is denoted with ϵ_1.

(2) A second, brief non-slow-roll epoch lasting between two conformal times τ_1 and τ_2. The parameter η is negative and large in absolute magnitude, while the small, time dependent parameter $\epsilon(\tau)$ rapidly decreases (and the Hubble parameter remains almost constant).

(3) Finally, a third era of slow-roll evolution for $\tau_2 \leq \tau \leq 0$, where ϵ and η are both small and constant. The value of the parameter ϵ in this phase is denoted with ϵ_2.

We rescale the curvature perturbation $\zeta_k(\tau)$ as

$$\varphi_k(\tau) = z(\tau)\zeta_k(\tau). \tag{A1}$$

The Mukhanov-Sasaki equation for the variable $\varphi_k(\tau)$ reads

$$\varphi_k''(\tau) + \left(k^2 - \frac{z''(\tau)}{z(\tau)}\right)\varphi_k(\tau) = 0. \tag{A2}$$

The general expression of the pump field $z(\tau)$ is

$$z(\tau) = a(\tau)\sqrt{2\epsilon(\tau)}. \tag{A3}$$

Given the conditions described above, in a quasi–de Sitter limit the pump field can be parametrized as follows:

$$z(\tau) = \begin{cases} -\frac{\sqrt{2\epsilon_1}}{H_0\tau} & \text{for } \tau \leq \tau_1 \\ -\frac{\sqrt{2\epsilon(\tau)}}{H_0\tau} & \text{for } \tau_1 \leq \tau \leq \tau_2 \\ -\frac{\sqrt{2\epsilon_2}}{H_0\tau} & \text{for } \tau_2 \leq \tau \leq 0 \end{cases} \tag{A4}$$

with $\epsilon(\tau)$ a continuous function, and H_0 the (nearly constant) Hubble parameter during inflation. We define the parameter η as

$$\eta = -\lim_{\tau \to \tau_1^+} \frac{d\ln\epsilon(\tau)}{d\ln\tau}, \tag{A5}$$

and we consider it constant, negative, and large in absolute value.

We parametrize the solution of the Mukhanov-Sasaki equation (A2) in terms of the following formal series:

$$\varphi_k(\tau) = -i\frac{H_0 e^{-ik\tau}}{2\sqrt{\epsilon_1 k^3}}z(\tau)[1 + ik\tau + (ik\tau_1)^2 A_{(2)}(\tau) + (ik\tau_1)^3 A_{(3)}(\tau) + \cdots], \tag{A6}$$

where the functions $A_{(n)}(\tau)$, $n \geq 2$, have to be determined. Plugging the ansatz (A6) into the Mukhanov Sasaki equation (A2), we find the following coupled system of equations for the quantities $A_n(\tau)$:

$$\left[\frac{\epsilon(\tau)}{\tau^2}\tau_1^2 A'_{(2)}(\tau)\right]' = \frac{\epsilon'(\tau)}{\tau}, \tag{A7}$$

$$\left[\frac{\epsilon(\tau)}{\tau^2}(\tau_1 A'_{(n)}(\tau) - A_{(n-1)}(\tau))\right]' = \frac{\epsilon(\tau)A'_{(n-1)}(\tau)}{\tau^2}, \quad \text{for } n > 2. \tag{A8}$$

If $\epsilon(\tau)$ is constant, then a consistent solution is $A_{(n)} = 0$ for $n \geq 2$, and Eq. (A6) reduces to the usual solution for mode functions in the de Sitter limit. But we are interested in evaluating the effects of a time dependent $\epsilon(\tau)$ (and a large η parameter) during the non-slow-roll phase of evolution. A formal solution for Eq. (A7) is

$$\tau_1^2 A_{(2)}(\tau) = \int_{-\infty}^{\tau} d\tau_a \frac{\tau_a^2}{\epsilon(\tau_a)}\left(\int_{-\infty}^{\tau_a} d\tau_b \frac{\epsilon'(\tau_b)}{\tau_b}\right). \tag{A9}$$

For $\tau < \tau_1$, the ϵ parameter is constant and $A_{(2)}(\tau)$ vanishes as desired: it acquires a nonzero value starting from $\tau = \tau_1$ onwards.

Considering values of $A_{(n)}(\tau)$ for $n > 2$, we find the following formal solution for Eq. (A8):

$$\tau_1 A_{(n)}(\tau) = \int_{-\infty}^{\tau} d\tau_a A_{(n-1)}(\tau_a) + \int_{-\infty}^{\tau} d\tau_a \frac{\tau_a^2}{\epsilon(\tau_a)}\left(\int_{-\infty}^{\tau_a} d\tau_b \frac{\epsilon(\tau_b)A'_{(n-1)}(\tau_b)}{\tau_b^2}\right). \tag{A10}$$

Interestingly, we can now exploit the fact that the duration of the non-slow-roll phase is small, $-(\tau_2 - \tau_1)/\tau_1 \ll 1$. We expand in Taylor series the previous formal solutions, focusing on the leading term (more details in [18]). For $A_{(2)}$ we find, when evaluated at $\tau_1 \leq \tau \leq \tau_2$,

$$A_{(2)}(\tau) = \left(\frac{d\ln\epsilon(\tau)}{d\ln\tau}\right)_{\tau=\tau_1}\frac{(\tau-\tau_1)^2}{\tau_1^2} + \mathcal{O}[(\tau-\tau_1)^3],$$

$$= -\eta\frac{1}{2}\frac{(\tau-\tau_1)^2}{\tau_1^2} + \mathcal{O}[(\tau-\tau_1)^3]. \tag{A11}$$

Proceeding analogously and Taylor expanding for higher n, we find the following leading contributions:

$$A_{(n)}(\tau) = -\eta\frac{2^{n-2}}{n!}\frac{(\tau-\tau_1)^n}{\tau_1^n}, \quad \text{for } n \geq 2. \tag{A12}$$

Plugging the solutions of Eq. (A12) into Eq. (A6), one finds an exponential series, which can be resummed giving

$$\varphi_k(\tau) = -i\frac{H_0 e^{-ik\tau}}{2\sqrt{\epsilon_1 k^3}} z(\tau)\left[1 + ik\tau + \frac{\eta}{4}\left(1 + 2ik(\tau - \tau_1) - e^{2ik(\tau-\tau_1)}\right)\right] \qquad \text{for } \tau_1 \leq \tau \leq \tau_2. \tag{A13}$$

This expression, valid for $\tau \leq \tau_2$, can then be matched to a solution of the Mukhanov-Sasaki equation in the interval $\tau_2 \leq \tau \leq 0$. Recall that in this epoch we return to a slow-roll regime where ϵ and η are negligibly small; hence, the most general solution for the mode function is

$$\varphi_k(\tau) = -i\mathcal{K}_1\frac{H_0 e^{-ik\tau}}{2\sqrt{\epsilon_1 k^3}} z(\tau)(1 + ik\tau) - i\mathcal{K}_2\frac{H_0 e^{ik\tau}}{2\sqrt{\epsilon_1 k^3}} z(\tau)(1 - ik\tau). \tag{A14}$$

The scale-dependent quantities $\mathcal{K}_{1,2}$ are determined by Israel matching the expression (A14) with the solution (A6) at time τ_2. Defining $\Delta\tau = -(\tau_2 - \tau_1)/\tau_1$, the result is

$$\mathcal{K}_1 = 1 - \frac{\eta}{8(1 - \Delta\tau)^2 k^2 \tau_1^2}\left[1 - e^{-2ik\tau_1\Delta\tau} + k\tau_1\Delta\tau(i + 2k\tau_1(1 - \Delta\tau))\right], \tag{A15}$$

$$\mathcal{K}_2 = \frac{\eta e^{-2ik\tau_1(1-\Delta\tau)}}{8(1 - \Delta\tau)^2 k^2 \tau_1^2}\left[1 + 2ik\tau_1 - e^{-2ik\tau_1\Delta\tau}(i + 2k\tau_1(1 - \Delta\tau))\right]. \tag{A16}$$

It is straightforward to compute the two point function for curvature perturbations at the end of inflation $\tau = 0$ in terms of $|\varphi_k(\tau)|^2$ using Eqs. (A14)–(A16). The result can be used to prove Eq. (2.11) in the main text (see also [18]). Taking the large $|\eta|$ limit following Eq. (2.3), one recovers the expression (2.5) in the main text [expressed in terms of the dimensionless momenta κ defined in Eq. (2.4)].

APPENDIX B: EXPLICIT EXPRESSIONS FOR THE COEFFICIENTS $\mathcal{C}_n$

In this Appendix we collect the explicit functions $\mathcal{C}_n$, $n = 1, ...4$, which form the analytic scalar bispectrum of Eq. (3.9). After defining

$$\Delta_{pq} = 1 + \delta_{pq}, \quad \Delta_{pqr} = (1 + \delta_{pq})(1 + \delta_{qr} + \delta_{pr}), \tag{B1}$$

we make use of the convenient combinations

$$K_p = \sum_i k_i^p, \tag{B2}$$

$$K_{pq} = \frac{1}{\Delta_{pq}}\sum_{i\neq j} k_i^p k_j^q, \tag{B3}$$

$$K_{pqr} = \frac{1}{\Delta_{pqr}}\sum_{i\neq j\neq \ell} k_i^p k_j^q k_\ell^r, \tag{B4}$$

introduced in [121]. The previous combinations allow us to express the functions $\mathcal{C}_n$ as

$$\mathcal{C}_1 = \frac{(K_{114} + 3K_{123} + 6K_{222} - K_4 - 2K_{13} - 2K_{22} - 2K_{112})}{K_{333}} j_1(\kappa_1 + \kappa_2 + \kappa_3)$$
$$+ \frac{(K_{14} + 3K_{23} + 2K_{113} + 2K_{112})}{K_{333}} j_0(\kappa_1 + \kappa_2 + \kappa_3) \tag{B5}$$

$$\mathcal{C}_2 = \frac{1}{K_{444}}[10K_{134} + 14K_{233} + 9K_{224} + 2K_{125} - K_{112} - K_{13}$$
$$- K_{24} - 3K_{222} - K_{15} - 2K_{123} - 3K_{114}]j_0(\kappa_1 + \kappa_2 + \kappa_3)$$
$$+ \frac{1}{K_{444}}[K_{225} + 7K_{234} + 18K_{333} + 3K_{113} + 2K_{122} + K_{23}$$
$$- 12K_{113} - 3K_{115} - 9K_{124} - 13K_{223} - K_{25} - 3K_{34}]j_1(\kappa_1 + \kappa_2 + \kappa_3)$$

$$+ \frac{1}{K_{333}} \left\{ [K_2 + K_{13} + K_4 - (2K_3 + K_{12})\kappa_3 \right.$$

$$+ (K_2 + K_{11} + K_4 - K_{13} - 4K_{22})\kappa_3^2 + (2K_3 + 2K_{12} - 2K_1 + 2)\kappa_3^3$$

$$+ (1 + K_{11} + 2K_2)\kappa_3^5 - 2K_1\kappa_3^5 - 3\kappa_3^6] \frac{j_0(\kappa_1 + \kappa_2 - \kappa_3)}{\kappa_3} + \text{perms} \right\}$$

$$+ \left\{ [K_{14} + 3K_{23} - K_{12} - K_3 + (2K_2 - 2K_{22} - K_4 - K_{13})\kappa_3 \right.$$

$$+ (2K_{12} - K_3 + 3K_{23} + K_{14})\kappa_3^2 + (2K_{22} + K_{13} - K_4 - 4K_2 - K_{11})\kappa_3^3$$

$$- (K_{12} + 4K_3 + 2K_1)\kappa_3^4 + (9 - K_{11} - 4K_2)\kappa_3^5 + 9\kappa_3^7] \frac{j_1(\kappa_1 + \kappa_2 - \kappa_3)}{\kappa_3} + \text{perms} \right\}$$

$$\mathcal{C}_3 = \frac{4(18K_{122} + 2K_{113} - 3K_{12} - 3K_3)}{3K_{222}} j_1(\kappa_1) j_1(\kappa_2) j_1(\kappa_3)$$

$$+ \left[\frac{8(\kappa_3^3 K_1 + 2\kappa_3^2 K_2 - \kappa_3 K_{12} - 3\kappa_3^4)}{K_{222}} j_1(\kappa_1) j_1(\kappa_2) j_0(\kappa_3) + \text{perms} \right] \tag{B6}$$

$$\mathcal{C}_4 = \frac{16K_{11}}{K_{111}} j_1(\kappa_1) j_1(\kappa_2) j_1(\kappa_3), \tag{B7}$$

where $j_{0,1}$ are spherical Bessel functions [see Eq. (2.10)]. The resulting bispectrum has a rich shape and scale dependence, as discussed in the main text.

APPENDIX C: COMPUTATION OF THE TENSOR-TENSOR-SCALAR BISPECTRUM

In this Appendix we evaluate the tensor-tensor-scalar bispectrum B_{TTS} during radiation domination. Tensor modes are sourced at second order in perturbations by scalar fluctuations, which are enhanced at small scales by the non-slow-roll epoch described in Secs. II and III. This is a well studied phenomenon, and explicit semianalytic formulas for computing the properties of the induced tensor modes have been developed—see, e.g., [58,59,120]. We make use and develop previous results (especially [59]) to compute the observable B_{TTS} during radiation domination. For convenience, here we make use of dimensionful momenta $\vec{k}$ (their dimensionless version used in the main text can be easily obtained as $\vec{\kappa} = -\tau_1 \vec{k}$).

The Fourier transform of tensor modes sourced by scalar fluctuations is

$$h_{\vec{k}}(\tau) = \frac{1}{a(\tau)} \int d\tilde{\tau} g_k(\tau, \tilde{\tau}) [a(\tilde{\tau}) S(\tilde{\tau}, \vec{k})], \tag{C1}$$

where $g_k(\tau, \tilde{\tau})$ is a Green function. In radiation domination it is given by

$$g_k(\tau, \tilde{\tau}) = \frac{1}{k} (\sin(k\tau) \sin(k\tilde{\tau}) - \cos(k\tau) \cos(k\tilde{\tau})). \tag{C2}$$

The source contribution $S(\tau, \vec{k})$ is given by a convolution integral involving scalar fluctuations [59]

$$S(\tau, \vec{k}) = \int d^3 q \mathbf{e}(\vec{k}, \vec{q}) f(\tau, \vec{k}, \vec{q}) \zeta_{\vec{k}-\vec{q}} \zeta_{\vec{q}}. \tag{C3}$$

The curvature fluctuations appearing in Eq. (C3) are primordial perturbations evaluated right at the end of inflation, $\tau = 0$. The quantity $\mathbf{e}(\vec{k}, \vec{q})$ originates from contractions of polarization tensors. It is given by

$$\mathbf{e}(\vec{k}, \vec{q}) = q^2 - \frac{(\vec{q} \cdot \vec{k})^2}{k^2}, \tag{C4}$$

and it has the property $\mathbf{e}(\vec{k}, \vec{k} - \vec{q}) = \mathbf{e}(\vec{k}, \vec{q})$. The quantity f controls propagation effects from the end of inflation to time $\tau > 0$ during radiation domination. In absence of anisotropic stress it is given by [58]

$$f(\tau, \vec{k}, \vec{q}) = \left[12\Phi(\tau|\vec{k} - \vec{q}|)\Phi(\tau|\vec{q}|) + \left(\tau\Phi(\tau|\vec{k} - \vec{q}|) + \frac{\tau^2}{2}\Phi'(\tau|\vec{k} - \vec{q}|) \right)\Phi'(\tau|\vec{q}|) \right]. \tag{C5}$$

In fact, the Bardeen scalar potential $\Phi_{\vec{k}}(\tau)$ during radiation domination is related to the curvature perturbation at the end of inflation $\zeta_{\vec{k}}$ by the transfer function

$$\Phi_{\vec{k}}(\tau) = \Phi(k\tau)\zeta_{\vec{k}}, \tag{C6}$$

with

$$\Phi(k\tau) = \frac{2}{(k\tau)^2}\left(\frac{\sqrt{3}\sin{(k\tau/\sqrt{3})}}{k\tau} - \cos{(k\tau/\sqrt{3})}\right). \tag{C7}$$

The transfer function has the limit $\Phi(k\tau) \to 2/3$ when its argument tends to zero.

By means of these quantities it is straightforward to compute n-point functions involving tensor and/or scalar fluctuations. The two point function of tensor modes reads $(0 \le \tau \le \tau_2)$

$$\langle h_{\vec{k}_1}(\tau)h_{\vec{k}_2}(\tau)\rangle = \frac{1}{a^2(\tau)}\int_{\tau_0}^{\tau}d\tau_2\int_{\tau_0}^{\tau}d\tau_1 a(\tau_1)a(\tau_2)g_{\vec{k}_1}(\tau,\tau_1)g_{\vec{k}_2}(\tau,\tau_2)\langle S(\tau_1,\vec{k}_1)S(\tau_2,\vec{k}_2)\rangle. \tag{C8}$$

While the three point function with two tensors and one scalar mode results

$$\langle h_{\vec{k}_1}(\tau)h_{\vec{k}_2}(\tau)\Phi_{\vec{k}_3}(\tau)\rangle = \frac{\Phi(k_3\tau)}{a^2(\tau)}\int_{\tau_0}^{\tau}d\tau_2\int_{\tau_0}^{\tau}d\tau_1 a(\tau_1)a(\tau_2)g_{\vec{k}_1}(\tau,\tau_1)g_{\vec{k}_2}(\tau,\tau_2)\langle S(\tau_1,\vec{k}_1)S(\tau_2,\vec{k}_2)\zeta_{\vec{k}_3}\rangle. \tag{C9}$$

Using Wick's theorem, one finds

$$\langle S(\vec{k}_1,\tau_1)S(\vec{k}_2,\tau_2)\rangle = \delta(\vec{k}_1 + \vec{k}_2)\int d^3q_1(e(\vec{k}_1,\vec{q}_1))^2 f(\vec{k}_1,\vec{q}_1,\tau_1)[f(\vec{k}_1,\vec{q}_1,\tau_2) + f(\vec{k}_1,\vec{k}_1 - \vec{q}_1,\tau_2)]$$
$$\times P_\zeta(|\vec{k}_1 - \vec{q}_1|)P_\zeta(q_1), \tag{C10}$$

where the curvature power spectrum is defined in Eq. (2.6). Plugging the previous expression in Eq. (C8), we can determine the induced tensor spectrum. It can be expressed as the convolution

$$P_h(\tau, k) = \int d^3q P_\zeta(|\vec{k} - \vec{q}|)P_\zeta(q)\mathcal{F}_0(\tau, \vec{k}, \vec{q}), \tag{C11}$$

with

$$\mathcal{F}_0(\tau, \vec{k}, \vec{q}) = \frac{1}{a^2(\tau)}\int_{\tau_0}^{\tau}d\tau_2\int_{\tau_0}^{\tau}d\tau_1 a(\tau_1)a(\tau_2)g_k(\tau,\tau_1)g_k(\tau,\tau_2)(e(\vec{k},\vec{q}))^2 f(\vec{k},\vec{q},\tau_1)[f(\vec{k},\vec{q},\tau_2) + f(\vec{k},\vec{k}-\vec{q},\tau_2)]. \tag{C12}$$

The three point function in Eq. (C9) is more elaborated. An application of Wick theorem suggests to split the result in two separate convolution integrals:

$$\langle S(\tau_1,\vec{k}_1)S(\tau_2,\vec{k}_2)\zeta_{\vec{k}_3}\rangle = \delta(\vec{k}_1 + \vec{k}_2 + \vec{k}_3)(I_1 + I_2), \tag{C13}$$

with respectively

$$I_1 = \int d^3q_1[e(\vec{k}_1,\vec{q}_1)f(\vec{k}_1,\vec{q}_1,\tau_1)e(\vec{k}_1+\vec{k}_3,-\vec{q}_1+\vec{k}_1)f(-\vec{k}_3-\vec{k}_1,-\vec{k}_3-\vec{q}_1,\tau_2)$$
$$+ e(\vec{k}_1,\vec{q}_1)f(\vec{k}_1,\vec{q}_1,\tau_1)e(\vec{k}_1+\vec{k}_3,\vec{q}_1+\vec{k}_3)f(\vec{k}_1+\vec{k}_3,\vec{k}_1-\vec{q}_1,\tau_2)]$$
$$\times \mathcal{P}_\zeta(|\vec{k}_1 - \vec{q}_1|)B_\zeta(q_1,|\vec{k}_3+\vec{q}_1|,k_3), \tag{C14}$$

$$I_2 = e(\vec{k}_1,\vec{k}_1+\vec{k}_3)f(\vec{k}_1,\vec{k}_1+\vec{k}_3,\tau_1)P_\zeta(k_3)$$
$$\times \int d^3q_1 e(\vec{k}_1+\vec{k}_3,-\vec{q}_1)f(\vec{k}_1+\vec{k}_3,-\vec{q}_1,\tau_2)B_\zeta(|\vec{k}_1+\vec{k}_3|,|\vec{q}_1+\vec{k}_1+\vec{k}_3|,q_1). \tag{C15}$$

Accordingly, the B_{TTS} bispectrum results (with $\vec{k}_2 = -\vec{k}_1 - \vec{k}_3$):

$$B_{\text{TTS}}(\vec{k}_1, \vec{k}_2, \vec{k}_3) = \int d^3 q P_\zeta(|\vec{k}_1 - \vec{q}|) B_\zeta(q, |\vec{k}_3 + \vec{q}|, k_3) \mathcal{F}_1(\tau, \vec{k}_1, \vec{k}_3, \vec{q})$$

$$+ P_\zeta(k_3) \int d^3 q B_\zeta(|\vec{k}_1 + \vec{k}_3|, |\vec{q}_1 + \vec{k}_1 + \vec{k}_3|, q_1) \mathcal{F}_2(\tau, \vec{k}_1, \vec{k}_3, \vec{q}), \tag{C16}$$

with

$$\mathcal{F}_1(\tau, \vec{k}_1, \vec{k}_3, \vec{q}) = \frac{1}{a^2(\tau)} \int_{\tau_0}^\tau d\tau_2 \int_{\tau_0}^\tau d\tau_1 a(\tau_1) a(\tau_2) g_k(\tau, \tau_1) g_k(\tau, \tau_2)$$

$$\times [\mathbf{e}(\vec{k}_1, \vec{q}) f(\vec{k}_1, \vec{q}, \tau_1) \mathbf{e}(\vec{k}_1 + \vec{k}_3, -\vec{q} + \vec{k}_1) f(-\vec{k}_3 - \vec{k}_1, -\vec{k}_3 - \vec{q}, \tau_2)$$

$$+ \mathbf{e}(\vec{k}_1, \vec{q}) f(\vec{k}_1, \vec{q}, \tau_1) \mathbf{e}(\vec{k}_1 + \vec{k}_3, \vec{q} + \vec{k}_3) f(\vec{k}_1 + \vec{k}_3, \vec{k}_1 - \vec{q}, \tau_2)] \tag{C17}$$

$$\mathcal{F}_2(\tau, \vec{k}_1, \vec{k}_3, \vec{q}) = \frac{1}{a^2(\tau)} \int_{\tau_0}^\tau d\tau_2 \int_{\tau_0}^\tau d\tau_1 a(\tau_1) a(\tau_2) g_k(\tau, \tau_1) g_k(\tau, \tau_2)$$

$$\times [\mathbf{e}(\vec{k}_1, \vec{k}_1 + \vec{k}_3) f(\vec{k}_1, \vec{k}_1 + \vec{k}_3, \tau_1) \mathbf{e}(\vec{k}_1 + \vec{k}_3, -\vec{q}) f(\vec{k}_1 + \vec{k}_3, -\vec{q}, \tau_2)]. \tag{C18}$$

A considerable simplification occurs in the squeezed limit, when the momentum of the scalar perturbation $\vec{k}_3 \to 0$. In this regime the function $\mathcal{F}_2$ is suppressed by a small factor k_3^2 with respect to $\mathcal{F}_1$. The latter, moreover, becomes coincident to $\mathcal{F}_0$. Consequently, for $\vec{k}_3 \to 0$, we find the relation

$$\lim_{k_3 \to 0} B_{\text{TTS}}(k, k, k_3) = P_\zeta(k_3) \int d^3 q P_\zeta(|\vec{k} - \vec{q}|) P_\zeta(q) [1 - n_\zeta(q)] \mathcal{F}(\tau, \vec{k}, \vec{q}) \tag{C19}$$

whose interesting physical implications are considered in Sec. IV. The function $\mathcal{F}_0$ is introduced in Eq. (C12), and we used the fact that the scalar bispectrum satisfies the Maldacena consistency relation in the squeezed limit—Sec. III. Notice that, besides the squeezed limit above, our general formulas derived in this Appendix are exact and can be used to study other shapes of the tensor-tensor-scalar bispectrum during the radiation dominated era.

---

[1] S. Hawking, Gravitationally collapsed objects of very low mass, Mon. Not. R. Astron. Soc. **152,** 75 (1971).

[2] B. J. Carr and S. W. Hawking, Black holes in the early Universe, Mon. Not. R. Astron. Soc. **168,** 399 (1974).

[3] P. Ivanov, P. Naselsky, and I. Novikov, Inflation and primordial black holes as dark matter, Phys. Rev. D **50,** 7173 (1994).

[4] J. Garcia-Bellido, A. D. Linde, and D. Wands, Density perturbations and black hole formation in hybrid inflation, Phys. Rev. D **54,** 6040 (1996).

[5] M. Y. Khlopov, Primordial black holes, Res. Astron. Astrophys. **10,** 495 (2010).

[6] J. García-Bellido, Massive primordial black holes as dark matter and their detection with gravitational waves, J. Phys. Conf. Ser. **840,** 012032 (2017).

[7] M. Sasaki, T. Suyama, T. Tanaka, and S. Yokoyama, Primordial black holes—Perspectives in gravitational wave astronomy, Classical Quantum Gravity **35,** 063001 (2018).

[8] B. Carr and F. Kuhnel, Primordial black holes as dark matter: Recent developments, Annu. Rev. Nucl. Part. Sci. **70,** 355 (2020).

[9] A. M. Green and B. J. Kavanagh, Primordial black holes as a dark matter candidate, J. Phys. G **48,** 043001 (2021).

[10] A. Escrivà, F. Kuhnel, and Y. Tada, Primordial black holes, arXiv:2211.05767.

[11] O. Özsoy and G. Tasinato, Inflation and primordial black holes, arXiv:2301.03600.

[12] D. Baumann, Inflation, in *Theoretical Advanced Study Institute in Elementary Particle Physics: Physics of the Large and the Small* (World Scientific, 2011), pp. 523–686, https://www.worldscientific.com/worldscibooks/10.1142/7961#t=aboutBook.

[13] A. A. Starobinsky, Spectrum of adiabatic perturbations in the universe when there are singularities in the inflation potential, JETP Lett. **55,** 489 (1992).

[14] D. Wands, Duality invariance of cosmological perturbation spectra, Phys. Rev. D **60,** 023507 (1999).

[15] S. M. Leach, M. Sasaki, D. Wands, and A. R. Liddle, Enhancement of superhorizon scale inflationary curvature perturbations, Phys. Rev. D **64,** 023512 (2001).

[16] O. Özsoy and G. Tasinato, On the slope of the curvature power spectrum in non-attractor inflation, J. Cosmol. Astropart. Phys. 04 (2020) 048.

[17] P. Carrilho, K. A. Malik, and D. J. Mulryne, Dissecting the growth of the power spectrum for primordial black holes, Phys. Rev. D **100,** 103529 (2019).

[18] G. Tasinato, An analytic approach to non-slow-roll inflation, Phys. Rev. D **103,** 023535 (2021).

[19] G. Franciolini and A. Urbano, Primordial black hole dark matter from inflation: The reverse engineering approach, Phys. Rev. D **106,** 123519 (2022).

[20] A. Karam, N. Koivunen, E. Tomberg, V. Vaskonen, and H. Veermäe, Anatomy of single-field inflationary models for primordial black holes, J. Cosmol. Astropart. Phys. 03 (2023) 013.

[21] G. Domènech, G. Vargas, and T. Vargas, An exact model for enhancing/suppressing primordial fluctuations, arXiv:2309.05750.

[22] G. Tasinato, Large $|\eta|$ approach to single field inflation, Phys. Rev. D **108,** 043526 (2023).

[23] G. 't Hooft, A planar diagram theory for strong interactions, Nucl. Phys. **B72,** 461 (1974).

[24] S. Coleman, *Aspects of Symmetry: Selected Erice Lectures* (Cambridge University Press, Cambridge, England, 1985).

[25] J. Garcia-Bellido, M. Peloso, and C. Unal, Gravitational waves at interferometer scales and primordial black holes in axion inflation, J. Cosmol. Astropart. Phys. 12 (2016) 031.

[26] J. Garcia-Bellido, M. Peloso, and C. Unal, Gravitational wave signatures of inflationary models from primordial black hole dark matter, J. Cosmol. Astropart. Phys. 09 (2017) 013.

[27] J. M. Ezquiaga, J. García-Bellido, and V. Vennin, The exponential tail of inflationary fluctuations: Consequences for primordial black holes, J. Cosmol. Astropart. Phys. 03 (2020) 029.

[28] S. Pi and M. Sasaki, Primordial black hole formation in nonminimal curvaton scenarios, Phys. Rev. D **108,** L101301 (2023).

[29] Y.-F. Cai, X.-H. Ma, M. Sasaki, D.-G. Wang, and Z. Zhou, One small step for an inflaton, one giant leap for inflation: A novel non-Gaussian tail and primordial black holes, Phys. Lett. B **834,** 137461 (2022).

[30] S. Pi and M. Sasaki, Logarithmic duality of the curvature perturbation, Phys. Rev. Lett. **131,** 011002 (2023).

[31] R. Saito, J. Yokoyama, and R. Nagata, Single-field inflation, anomalous enhancement of superhorizon fluctuations, and non-Gaussianity in primordial black hole formation, J. Cosmol. Astropart. Phys. 06 (2008) 024.

[32] C. T. Byrnes, E. J. Copeland, and A. M. Green, Primordial black holes as a tool for constraining non-Gaussianity, Phys. Rev. D **86,** 043512 (2012).

[33] S. Young and C. T. Byrnes, Primordial black holes in non-Gaussian regimes, J. Cosmol. Astropart. Phys. 08 (2013) 052.

[34] E. V. Bugaev and P. A. Klimai, Primordial black hole constraints for curvaton models with predicted large non-Gaussianity, Int. J. Mod. Phys. D **22,** 1350034 (2013).

[35] S. Young and C. T. Byrnes, Signatures of non-Gaussianity in the isocurvature modes of primordial black hole dark matter, J. Cosmol. Astropart. Phys. 04 (2015) 034.

[36] G. Franciolini, A. Kehagias, S. Matarrese, and A. Riotto, Primordial black holes from inflation and non-Gaussianity, J. Cosmol. Astropart. Phys. 03 (2018) 016.

[37] S. Passaglia, W. Hu, and H. Motohashi, Primordial black holes and local non-Gaussianity in canonical inflation, Phys. Rev. D **99,** 043536 (2019).

[38] V. Atal and C. Germani, The role of non-Gaussianities in primordial black hole formation, Phys. Dark Universe **24,** 100275 (2019).

[39] M. Biagetti, G. Franciolini, A. Kehagias, and A. Riotto, Primordial black holes from inflation and quantum diffusion, J. Cosmol. Astropart. Phys. 07 (2018) 032.

[40] V. Atal, J. Garriga, and A. Marcos-Caballero, Primordial black hole formation with non-Gaussian curvature perturbations, J. Cosmol. Astropart. Phys. 09 (2019) 073.

[41] A. Kehagias, I. Musco, and A. Riotto, Non-Gaussian formation of primordial black holes: Effects on the threshold, J. Cosmol. Astropart. Phys. 12 (2019) 029.

[42] V. De Luca, G. Franciolini, A. Kehagias, M. Peloso, A. Riotto, and C. Ünal, The ineludible non-Gaussianity of the primordial black hole abundance, J. Cosmol. Astropart. Phys. 07 (2019) 048.

[43] S. Young, I. Musco, and C. T. Byrnes, Primordial black hole formation and abundance: Contribution from the non-linear relation between the density and curvature perturbation, J. Cosmol. Astropart. Phys. 11 (2019) 012.

[44] C. Germani and R. K. Sheth, Nonlinear statistics of primordial black holes from Gaussian curvature perturbations, Phys. Rev. D **101,** 063520 (2020).

[45] M. Kawasaki and H. Nakatsuka, Effect of nonlinearity between density and curvature perturbations on the primordial black hole formation, Phys. Rev. D **99,** 123501 (2019).

[46] C.-M. Yoo, J.-O. Gong, and S. Yokoyama, Abundance of primordial black holes with local non-Gaussianity in peak theory, J. Cosmol. Astropart. Phys. 09 (2019) 033.

[47] D. G. Figueroa, S. Raatikainen, S. Rasanen, and E. Tomberg, Non-Gaussian tail of the curvature perturbation in stochastic ultraslow-roll inflation: Implications for primordial black hole production, Phys. Rev. Lett. **127,** 101302 (2021).

[48] M. Taoso and A. Urbano, Non-Gaussianities for primordial black hole formation, J. Cosmol. Astropart. Phys. 08 (2021) 016.

[49] S. Hooshangi, M. H. Namjoo, and M. Noorbala, Rare events are nonperturbative: Primordial black holes from heavy-tailed distributions, Phys. Lett. B **834,** 137400 (2022).

[50] S. Young, Peaks and primordial black holes: The effect of non-Gaussianity, J. Cosmol. Astropart. Phys. 05 (2022) 037.

[51] G. Ferrante, G. Franciolini, A. Iovino, Jr., and A. Urbano, Primordial non-Gaussianity up to all orders: Theoretical aspects and implications for primordial black hole models, Phys. Rev. D **107,** 043520 (2023).

[52] A. D. Gow, H. Assadullahi, J. H. P. Jackson, K. Koyama, V. Vennin, and D. Wands, Non-perturbative non-Gaussianity and primordial black holes, Europhys. Lett. **142,** 49001 (2023).

[53] E. Tomberg, Stochastic constant-roll inflation and primordial black holes, arXiv:2304.10903.

[54] J.-P. Li, S. Wang, Z.-C. Zhao, and K. Kohri, Complete analysis of scalar-induced gravitational waves and primordial non-Gaussianities f_{NL} and g_{NL}, arXiv:2309.07792.

[55] G. Franciolini, A. Iovino, Jr., V. Vaskonen, and H. Veermae, Recent gravitational wave observation by pulsar

timing arrays and primordial black holes: The importance of non-Gaussianities, Phys. Rev. Lett. **131**, 201401 (2023).

[56] S. Matarrese, O. Pantano, and D. Saez, A general relativistic approach to the nonlinear evolution of collisionless matter, Phys. Rev. D **47**, 1311 (1993).

[57] S. Matarrese, O. Pantano, and D. Saez, General relativistic dynamics of irrotational dust: Cosmological implications, Phys. Rev. Lett. **72**, 320 (1994).

[58] K. N. Ananda, C. Clarkson, and D. Wands, The cosmological gravitational wave background from primordial density perturbations, Phys. Rev. D **75**, 123518 (2007).

[59] D. Baumann, P. J. Steinhardt, K. Takahashi, and K. Ichiki, Gravitational wave spectrum induced by primordial scalar perturbations, Phys. Rev. D **76**, 084019 (2007).

[60] R. Saito and J. Yokoyama, Gravitational wave background as a probe of the primordial black hole abundance, Phys. Rev. Lett. **102**, 161101 (2009); **107**, 069901(E) (2011).

[61] R. Saito and J. Yokoyama, Gravitational-wave constraints on the abundance of primordial black holes, Prog. Theor. Phys. **123**, 867 (2010); **126**, 351(E) (2011).

[62] J. R. Espinosa, D. Racco, and A. Riotto, A cosmological signature of the SM Higgs instability: Gravitational waves, J. Cosmol. Astropart. Phys. 09 (2018) 012.

[63] G. Domènech, Induced gravitational waves in a general cosmological background, Int. J. Mod. Phys. D **29**, 2050028 (2020).

[64] V. De Luca, G. Franciolini, A. Kehagias, and A. Riotto, On the gauge invariance of cosmological gravitational waves, J. Cosmol. Astropart. Phys. 03 (2020) 014.

[65] K. Inomata and T. Terada, Gauge independence of induced gravitational waves, Phys. Rev. D **101**, 023523 (2020).

[66] G. Domènech, Scalar induced gravitational waves review, Universe **7**, 398 (2021).

[67] R.-g. Cai, S. Pi, and M. Sasaki, Gravitational waves induced by non-Gaussian scalar perturbations, Phys. Rev. Lett. **122**, 201101 (2019).

[68] C. Unal, Imprints of primordial non-Gaussianity on gravitational wave spectrum, Phys. Rev. D **99**, 041301 (2019).

[69] C. Yuan and Q.-G. Huang, Gravitational waves induced by the local-type non-Gaussian curvature perturbations, Phys. Lett. B **821**, 136606 (2021).

[70] V. Atal and G. Domènech, Probing non-Gaussianities with the high frequency tail of induced gravitational waves, J. Cosmol. Astropart. Phys. 06 (2021) 001; 10 (2023) E01.

[71] P. Adshead, K. D. Lozanov, and Z. J. Weiner, Non-Gaussianity and the induced gravitational wave background, J. Cosmol. Astropart. Phys. 10 (2021) 080.

[72] Z. Chang, Y.-T. Kuang, X. Zhang, and J.-Z. Zhou, Primordial black holes and third order scalar induced gravitational waves, Chin. Phys. C **47**, 055104 (2023).

[73] S. Garcia-Saenz, L. Pinol, S. Renaux-Petel, and D. Werth, No-go theorem for scalar-trispectrum-induced gravitational waves, J. Cosmol. Astropart. Phys. 03 (2023) 057.

[74] J.-P. Li, S. Wang, Z.-C. Zhao, and K. Kohri, Primordial non-Gaussianity f_{NL} and anisotropies in scalar-induced gravitational waves, J. Cosmol. Astropart. Phys. 10 (2023) 056.

[75] P. Adshead, N. Afshordi, E. Dimastrogiovanni, M. Fasiello, E. A. Lim, and G. Tasinato, Multimessenger cosmology: Correlating cosmic microwave background and stochastic gravitational wave background measurements, Phys. Rev. D **103**, 023532 (2021).

[76] S. Maity, H. V. Ragavendra, S. K. Sethi, and L. Sriramkumar, Loop contributions to the scalar power spectrum due to quartic order action in ultra-slow-roll inflation, arXiv:2307.13636.

[77] J. Kristiano and J. Yokoyama, Ruling out primordial black hole formation from single-field inflation, arXiv:2211.03395.

[78] J. Kristiano and J. Yokoyama, Response to criticism on "Ruling Out Primordial Black Hole Formation From Single-Field Inflation": A note on bispectrum and one-loop correction in single-field inflation with primordial black hole formation, arXiv:2303.00341.

[79] A. Riotto, The primordial black hole formation from single-field inflation is not ruled out, arXiv:2301.00599.

[80] S. Choudhury, M. R. Gangopadhyay, and M. Sami, No-go for the formation of heavy mass primordial black holes in single field inflation, arXiv:2301.10000.

[81] S. Choudhury, S. Panda, and M. Sami, No-go for PBH formation in EFT of single field inflation, arXiv:2302.05655.

[82] A. Riotto, The primordial black hole formation from single-field inflation is still not ruled out, arXiv:2303.01727.

[83] S. Choudhury, S. Panda, and M. Sami, Quantum loop effects on the power spectrum and constraints on primordial black holes, arXiv:2303.06066.

[84] H. Firouzjahi, One-loop corrections in power spectrum in single field inflation, arXiv:2303.12025.

[85] H. Motohashi and Y. Tada, Squeezed bispectrum and one-loop corrections in transient constant-roll inflation, arXiv:2303.16035.

[86] S. Choudhury, S. Panda, and M. Sami, Galileon inflation evades the no-go for PBH formation in the single-field framework, arXiv:2304.04065.

[87] H. Firouzjahi and A. Riotto, Primordial black holes and loops in single-field inflation, arXiv:2304.07801.

[88] H. Firouzjahi, Loop corrections in gravitational wave spectrum in single field inflation, arXiv:2305.01527.

[89] G. Franciolini, A. Iovino, Jr., M. Taoso, and A. Urbano, One loop to rule them all: Perturbativity in the presence of ultra-slow-roll dynamics, arXiv:2305.03491.

[90] J. Fumagalli, S. Bhattacharya, M. Peloso, S. Renaux-Petel, and L. T. Witkowski, One-loop infrared rescattering by enhanced scalar fluctuations during inflation, arXiv:2307.08358.

[91] Y. Tada, T. Terada, and J. Tokuda, Cancellation of quantum corrections on the soft curvature perturbations, arXiv:2308.04732.

[92] H. Firouzjahi, Revisiting loop corrections in single field USR inflation, arXiv:2311.04080.

[93] W. H. Kinney, Horizon crossing and inflation with large eta, Phys. Rev. D **72**, 023515 (2005).

[94] J. Martin, H. Motohashi, and T. Suyama, Ultra-slow-roll inflation and the non-Gaussianity consistency relation, Phys. Rev. D **87**, 023514 (2013).

[95] K. Dimopoulos, Ultra-slow-roll inflation demystified, Phys. Lett. B **775**, 262 (2017).

[96] H. Motohashi, A. A. Starobinsky, and J. Yokoyama, Inflation with a constant rate of roll, J. Cosmol. Astropart. Phys. 09 (2015) 018.

[97] S. Inoue and J. Yokoyama, Curvature perturbation at the local extremum of the inflaton's potential, Phys. Lett. B **524,** 15 (2002).

[98] K. Tzirakis and W. H. Kinney, Inflation over the hill, Phys. Rev. D **75,** 123510 (2007).

[99] K. Inomata, E. McDonough, and W. Hu, Amplification of primordial perturbations from the rise or fall of the inflaton, J. Cosmol. Astropart. Phys. 02 (2022) 031.

[100] C. T. Byrnes, P. S. Cole, and S. P. Patil, Steepest growth of the power spectrum and primordial black holes, J. Cosmol. Astropart. Phys. 06 (2019) 028.

[101] J. M. Maldacena, Non-Gaussian features of primordial fluctuations in single field inflationary models, J. High Energy Phys. 05 (2003) 013.

[102] M. H. Namjoo, H. Firouzjahi, and M. Sasaki, Violation of non-Gaussianity consistency relation in a single field inflationary model, Europhys. Lett. **101,** 39001 (2013).

[103] X. Chen, H. Firouzjahi, M. H. Namjoo, and M. Sasaki, A single field inflation model with large local non-Gaussianity, Europhys. Lett. **102,** 59001 (2013).

[104] X. Chen, Running non-Gaussianities in DBI inflation, Phys. Rev. D **72,** 123518 (2005).

[105] C. T. Byrnes, S. Nurmi, G. Tasinato, and D. Wands, Scale dependence of local fNL, J. Cosmol. Astropart. Phys. 02 (2010) 034.

[106] C. T. Byrnes, M. Gerstenlauer, S. Nurmi, G. Tasinato, and D. Wands, Scale-dependent non-Gaussianity probes inflationary physics, J. Cosmol. Astropart. Phys. 10 (2010) 004.

[107] P. Creminelli, A. Perko, L. Senatore, M. Simonović, and G. Trevisan, The physical squeezed limit: Consistency relations at order q^2, J. Cosmol. Astropart. Phys. 11 (2013) 015.

[108] O. Özsoy and G. Tasinato, CMB μT cross correlations as a probe of primordial black hole scenarios, Phys. Rev. D **104,** 043526 (2021).

[109] O. Özsoy and G. Tasinato, Consistency conditions and primordial black holes in single field inflation, Phys. Rev. D **105,** 023524 (2022).

[110] D. Babich, P. Creminelli, and M. Zaldarriaga, The shape of non-Gaussianities, J. Cosmol. Astropart. Phys. 08 (2004) 009.

[111] A. Malhotra, E. Dimastrogiovanni, G. Domènech, M. Fasiello, and G. Tasinato, New universal property of cosmological gravitational wave anisotropies, Phys. Rev. D **107,** 103502 (2023).

[112] E. Dimastrogiovanni, M. Fasiello, A. Malhotra, and G. Tasinato, Enhancing gravitational wave anisotropies with peaked scalar sources, J. Cosmol. Astropart. Phys. 01 (2023) 018.

[113] P. Auclair *et al.* (LISA Cosmology Working Group), Cosmology with the laser interferometer space antenna, Living Rev. Relativity **26,** 5 (2023).

[114] E. Dimastrogiovanni, M. Fasiello, and L. Pinol, Primordial stochastic gravitational wave background anisotropies: In-in formalization and applications, J. Cosmol. Astropart. Phys. 09 (2022) 031.

[115] E. Dimastrogiovanni, M. Fasiello, A. Malhotra, P. D. Meerburg, and G. Orlando, Testing the early universe with anisotropies of the gravitational wave background, J. Cosmol. Astropart. Phys. 02 (2022) 040.

[116] M. Braglia and S. Kuroyanagi, Probing prerecombination physics by the cross-correlation of stochastic gravitational waves and CMB anisotropies, Phys. Rev. D **104,** 123547 (2021).

[117] A. Ricciardone, L. V. Dall'Armi, N. Bartolo, D. Bertacca, M. Liguori, and S. Matarrese, Cross-correlating astrophysical and cosmological gravitational wave backgrounds with the cosmic microwave background, Phys. Rev. Lett. **127,** 271301 (2021).

[118] A. Malhotra, E. Dimastrogiovanni, M. Fasiello, and M. Shiraishi, Cross-correlations as a diagnostic tool for primordial gravitational waves, J. Cosmol. Astropart. Phys. 03 (2021) 088.

[119] G. Orlando, Probing parity-odd bispectra with anisotropies of GW V modes, J. Cosmol. Astropart. Phys. 12 (2022) 019.

[120] K. Kohri and T. Terada, Semianalytic calculation of gravitational wave spectrum nonlinearly induced from primordial curvature perturbations, Phys. Rev. D **97,** 123532 (2018).

[121] J. R. Fergusson and E. P. S. Shellard, The shape of primordial non-Gaussianity and the CMB bispectrum, Phys. Rev. D **80,** 043510 (2009).